Meteorological inventory of Rain-On-Snow events and detection assessment in the Canadian Arctic Archipelago using passive microwave radiometry

DOLANT C., [1,2] LANGLOIS A. [1,2], BRUCKER L.[3,4], ROYER A. [1,2], ROY A. [1,2], AND MONTPETIT B. [1]

ABSTRACT

The Arctic has witnessed significant warming over the past four decades, leading to a variability of consequences such as heat waves, increased occurrence of winter storms and rain-on-snow events (ROS). The spatial and temporal distributions of ROS across the Canadian Arctic Archipelago (CAA) remain poorly understood owing to their sporadic nature in time and space, which motivated the development of remote sensing algorithms. The potential of passive microwave observations was demonstrated in detecting ROS events. Lately, promising results were obtained using an algorithm based a brightness temperature gradient ratio. Its validation however remained limited due to a short study period and limited number of sites. This paper uses a large meteorological dataset across the CAA to further adapt our existing algorithm. Hence, this study highlights the distribution and evolution of ROS occurrences reported since 1985 at 14 Environment and Climate Change Canada (ECCC) weather stations across the CAA. Data show that more than 600 ROS events were inventoried since 1985, 80% of which occurred during the spring season. We introduce an adaptation of a detection algorithm (by sensitivity analysis on the detection threshold) with an error of ~5%, to investigate spatiotemporal patterns in event occurrence across the CAA.

Keywords: Rain-on-snow events; Canadian Arctic Archipelago (CAA); climatological trends; microwave radiometry

INTRODUCTION

The impacts of global climate change on the environment are significant due to a variety of climate feedback processes, such as an increased occurrence of heat waves, winter storms (Trenberth et al., 2007; Trenberth, 2011) and rain-on-snow (ROS) events (Brown and Mote, 2009; Chen et al. 2013). This is especially true in northern regions, where the warming is most pronounced (Serreze et al. 2009; Liston and Hiemstra, 2011; Serreze and Barry, 2011; Pradhanang et al. 2012 & 2013; Klos et al. 2014; Cullather et al. 2016). Direct consequences in the northern hemisphere include an overall reduction of snow depths (Brown and Braaten, 1998), snow cover extent (Brown et al. 2010; Derksen and Brown, 2012; Derksen et al., 2012) and sea ice extent (Steele et al. 2008; Holland et

[1] Centre d'Application et de Recherches en Télédétection, Université de Sherbrooke, Qc, Canada
[2] Centre for Northern Studies, Qc, Canada
[3] NASA Goddard Space Flight Center, Cryospheric Sciences Laboratory, Greenbelt, MD 20771, USA
[4] Universities Space Research Association, Goddard Earth Sciences Technology and Research Studies and Investigations, Columbia, MD 21044, USA

al. 2010; 2014; Comiso J.C, 2014), and an increased occurrence of extreme winter events (Grassi et al., 2013). More specifically, the rise in temperatures (L'hôte, 2005) has significant impacts on the precipitation regime (phase) and is amongst the most significant consequences of atmospheric warming and variability in the Arctic since the early 1980s (Winton, 2006; Liston and Hiemstra, 2011; IPCC, 2007 & 2014; Langlois et al. 2017). Of note, under warming temperature trends, ROS events on the one hand could increase with increasing ratio of rain versus snowfall events while on the other hand could decrease if the snow cover decreases. Such competitive impacts may render the trend of ROS difficult to analyse (Chen et al., 2015; Ye et al., 2008). However, from ROS-altered snow state analysis using satellite data, ROS events appear now more frequent than during the 1990s (Langlois et al. 2017) ROS significantly alters the snowpack state. Firstly, it leads to an increased liquid water content (LWC) in the snowpack. This process when followed by low air temperatures can then be responsible for the formation of ice crusts (Montpetit et al. 2013; Montpetit, 2015; Dolant et al. 2016) that have a strong impact on ecology (e.g., ungulate grazing conditions) (Putkonen and Roe, 2003; Rennert et al. 2009; Bokhorst et al. 2016; Johnson et al. 2016; Sokolov et al. 2016; Langlois et al. 2017; Ouellet et al. 2017), hydrology (e.g., modification of flow, soil saturation), and energy balance (e.g., modification of snow and soil surface and permafrost) (Putkonen, 1998; Dethloff et al. 2006; Mazurkiewicz et al., 2008; Romanovsky et al. 2010). ROS can also impact the snow surface properties (e.g., albedo) and the properties of the snow layers, such as density (Marshall et al., 1999), liquid water content and thermal conductivity (Domine et al., 2016).

Detecting ROS events from space borne microwave radiometry has been the subject of several studies (Grenfell and Putkonen, 2008; Dolant et al., 2016; Langlois et al., 2017). The use of passive microwaves (PMW) makes it possible to obtain information on the different snowpack layers based on their dielectric response. This represents an interesting avenue for tracking and studying ROS events across the Arctic from space. Grenfell and Putkonen (2008) demonstrated the possibility of using PMW to monitor ROS from space with a combination of microwave brightness temperature (T_B) gradient and polarization ratios. Their study was about on a single ROS event on Banks Island, and the authors highlighted the need for more statistics-based research. This motivated the work by Dolant et al. (2016), who developed an empirical approach to detect ROS using the gradient ratio in both vertical and horizontal polarizations. That work was validated with ROS observations in Nunavik (northern Québec, Canada), but the validation remained spatially and temporally limited. More recently, Langlois et al. (2017) analyzed the occurrence of ROS and ice layers detected from PMW and the link between these occurrences and caribou populations. Their work included PMW signatures from 18 islands across the Canadian Arctic Archipelago (CAA), and suggested an adjustment to the threshold initially proposed in Dolant et al. (2016).

The objectives of this paper are: (1) to inventory and classify all ROS observations recorded by the network of Environment and Climate Change Canada meteorological stations in the CAA and conduct a statistical analysis on ROS occurrence trends; and (2) to use this new dataset of ROS observations to validate and adapt the gradient ratio threshold suggested by Dolant et al. (2016) and evaluate the best value minimizing omission and commission errors in an operational application.

STUDY SITES AND DATA

Meteorological data

Water daily amount

ECCC characterizes the liquid precipitation by raindrop size and velocity to distinguish between precipitation phases. Here, we only present information about phase distinction (i.e., drizzle, hail, snow, rain) and precipitation amount (cumulative of the day) (Fig. 1A). Liquid water particles are discriminated as rain when the raindrop diameter is larger than 0.5 mm. Raindrops are normally larger in size than drizzle particles (i.e., small water drops with a diameter less than 0.5mm, uniform precipitation), however the partial evaporation of rain drops can lead to confusion. Solid precipitation (i.e., snow, hail), which can also blend with liquid precipitation, was classified as ROS $_{mix}$ in this study. Precipitation amounts were measured in millimeters with a rain gauge sensor, and

values below 0.2 mm were classified as "Trace". Precipitation was also characterized by intensity, from low (precipitation rate less than or equal to 2.5 $mm.h^{-1}$) to heavy (precipitation rate equal to or greater than 7.5 $mm.h^{-1}$).

In our database, precipitation events had predominantly small water amount (Fig. 1A). In all four classes (ROS_{rain}, $ROS_{rain/drizzle}$, ROS_{mix} and $ROS_{Unclass}$), the median amount of precipitation is under 0.9 mm while the mean amount precipitation ranges between 1.3 mm and 2.1 mm. The lowest average precipitation was in Alert (AT) and Sachs Harbour (SH), with 0.78±0.63 mm and 0.82±1.78 mm of rain per event, respectively. The highest values (>3mm) were recorded in Pond Inlet (PI), Nanisivik (NK) and Kugaaruk (KK), with precipitation averages of 3.6±5.60, 3.7±3.15 and 4.64±4.33 mm of rain, respectively.

Air temperature

The station temperature data (Fig. 1B) includes four distinct measurements: dry thermometer, wet thermometer and daily maxima and minima thermometers. These measurements are accurate to one tenth of a degree Celsius. The air temperatures in Figure 1 were extracted and averaged during ROS events only (ROS_{rain}, $ROS_{rain/drizzle}$, ROS_{mix} and $ROS_{Unclass}$). For our study period, the results showed that ROS_{rain} was observed at temperatures of 1.41±2.14 °C while $ROS_{rain/drizzle}$, ROS_{mix} and $ROS_{Unclass}$, occurred at colder temperatures, 0.06±2.56 °C, -1.06±6.8 °C and -2.11±5.05 °C, respectively. When considering all four classes, the mean observed air temperature during ROS was 0.05±3.77 °C).

Snow depth measurement

Snow depth (Fig. 1C) was measured by a trained person at the station using a snow scale (cm), and hourly measurements were available. The minimum observed snow depth we used was 5 cm to limit the number of satellite observations over grid cells with partial snow cover. For our study period, the statistics for snow depth measurements are similar for the four classes: 17.7±14.4 mm, 16.1±12.1 mm, 20.5±15.0 mm and 17.5±13.9 mm for ROS_{rain}, $ROS_{rain/drizzle}$, ROS_{mix} and $ROS_{Unclass}$ conditions, respectively.

Rain-on-Snow duration

The complementary observations recorded ROS event duration and precipitation type. An automatic system qualified the precipitation by state: rain, snow, drizzle, hail, freezing rain, freezing drizzle and unknown. We also extracted ROS event duration data. Results show ROS duration of 4.8±3.7 h, 6.0±4.3 h, 5.0±3.8 h and 2±0 h for the ROS_{rain}, $ROS_{rain/drizzle}$, ROS_{mix} and $ROS_{Unclass}$ conditions, respectively.

Data on precipitation intensity (low, moderate and heavy) was also available. Other information such as visibility and cloud conditions was available, but was not used in this study.

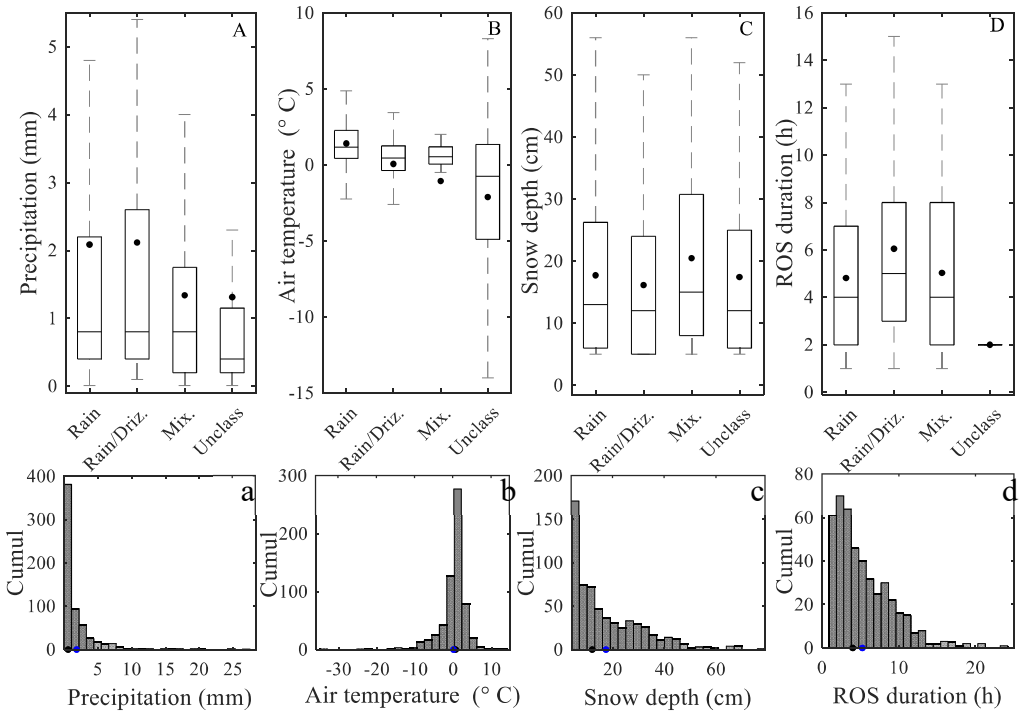

Figure 1. Statistics (upper row, labelled with capital letters) and distribution (lower row, labelled with lowercase letters) of precipitation amount (A,a), air temperature (B,b), snow depth (C,c) and ROS duration (D,d) measured at ECCC meteorological station. The values represent the average of all sites for four classes of ROS events. The boxplot (capital letter) represents interquartile range; black lines represent median and points represent mean value. The histograms (lowercase letters) show a distribution of ROS events (all classes); black points represent median value and blue points represent mean value.

Passive microwave data

For this study, time series of T_B were recorded by three passive microwave sensors onboard five different platforms between August 29, 1984 and June 18, 2014, and were downloaded from the National Snow and Ice Data Center (NSIDC) and used here for the ROS detection retrievals. The T_B dataset at 19 and 37 GHz in both horizontal H and vertical V polarizations was obtained from the Scanning Multichannel Microwave Radiometer (SMMR) (Knowles et al., 2000) onboard the Nimbus-7 platform for the period August 29, 1984 to July 9, 1987. After this period, the T_B was extracted from the Special Sensor Microwave/Imager (SSM/I) onboard Defense Meteorological Satellite Program (DMSP) satellite F08 from July 9, 1987 to December 6, 1991, and the SSM/I and the Special Sensor Microwave Imager/Sounder (SSMIS) (Wentz, 1997; Wentz and Spencer, 1998, Colton and Poe, 1999; Wentz, 2013) onboard DMSP F11, F13 and F17 from December 6, 1991 to June 18, 2014. The spatial resolution of these products is 25 km, projected on the Equal-Area Scalable Earth Grid (EASE-Grid). The products used consist of daily averages in EASE-Grid pixels for ascending and descending orbits $T_{B\ asc}$ and $T_{B\ desc}$). The ascending node is at local noon for SMMR, at 6:00 am for SSM/I F08 and 6:00 pm for T_B extracted from SSM/I and SSMI/S F11, F13 and F17 (local time). The descending node is offset by 12 hours.

METHODS

Inventory approach

Our inventory analysis focuses on the period 1984 (start of winter) to 2014 (end of winter), a period with coincident meteorological measurements (precipitation, air temperature, and snow depth) and human observations (qualitative information about precipitation type and ROS duration) from 14 ECCC stations across the CAA as well as daily passive microwave observations.

For each station and event during the analysis period, we extracted hourly measurement of precipitation amount, air temperature and snow depth values. Furthermore, in this study, four precipitation classes were analyzed: 1) precipitation composed of rain only ($ROS_{rain.}$); 2) precipitation composed of rain and drizzle ($ROS_{rain/drizzle}$); 3) precipitation composed of rain, hail and snow ($ROS_{mix.}$); and 4) rain with no specific observation of phase ($ROS_{Unclass}$). This classification is necessary to evaluate and enhance the detection capacity of our retrieval approach.

Atmospheric correction

An atmospheric correction is needed to remove atmospheric contribution in the satellite signal. Precipitable water data (PWAT) from the North American Regional Reanalysis (NARR) (Mesinger et al., 2006) was used to correct T_B data for atmospheric contributions (Roy et al., 2012). Atmospheric correction was calculated using the Millimeter-wave propagation model (Liebe, 1989) implemented in the Helsinki University of Technology (HUT) snow emission model (Pulliainen et al., 1999). The model considers radiative transfer through the atmospheric layers and calculates values of downwelling T_B ($T_{Batm\downarrow}$), atmospheric transmissivity (γ_{atm}) and atmospheric upwelling T_B ($T_{Batm\uparrow}$) (Liebe, 1989).

The relationship between PWAT and atmospheric upwelling contributions (adjusted from Roy, 2013) were expressed as follows:

$$T_{B_{atm}\uparrow(19)} = \left(0.879 \cdot PWAT\right) + 4.780 \quad (1)$$

$$T_{B_{atm}\uparrow(37)} = \left(0.602 \cdot PWAT\right) + 18.297 \quad (2)$$

The T_B corrected from the atmospheric contribution was obtained using Eq. (3):

$$T_{Bf\ corrected}^{\ pol} = T_{Bf\ raw}^{\ pol} \cdot \tau_f + T_{B_{atm}\uparrow f} \quad (3)$$

with

$$\tau_{(19)} = \left(-0.003 \cdot PWAT\right) + 0.979 \quad (4)$$

$$\tau_{(37)} = \left(-0.002 \cdot PWAT\right) + 0.924 \quad (5)$$

Over the CAA, the atmospheric corrections led to corrections averaging 1±0.4 K, 2±0.6 K, 1.6 ±0.4 K, 4±0.8 K for T_B at 19 GHz V and H and 37 GHz V and H, respectively.

Rain-On-Snow detection algorithm

The presence of liquid water within the snow and on its surface increases emissivity proportionally to frequency. As such, warm water at the surface (from a ROS event) will lead to a rapid increase of T_B at 37 GHz (faster than 19 GHz). Dolant et al. (2016) demonstrated that in the horizontal polarization, the T_B at 37 GHz becomes warmer than at 19 GHz, while 19 GHz in the vertical polarization remains warmer owing to a higher penetration depth (soil contributions). Dolant et al. (2016) demonstrated that the gradient ratio used by Grenfell and Putkonen (2008) in such conditions is positive in the vertical polarization and negative in the horizontal polarization.

$$GRP = \frac{T_{B37}^{\ v} - T_{B19}^{\ v}}{T_{B37}^{\ v} + T_{B19}^{\ v}} \cdot \frac{T_{B37}^{\ h} + T_{B19}^{\ h}}{T_{B37}^{\ h} - T_{B19}^{\ h}} \quad (6)$$

The ratio of gradient ratio, named GRP (Eq. 6), gives a signal inversion (negative GRP value) which characterizes rainfall. Dolant et al. (2016) demonstrated that a GRP threshold at 1 allowed for ROS detection in Nunavik, but it may be slightly too high for a larger scale application in the Arctic as considered in this paper.

RESULTS AND DISCUSSION

Rain-On-Snow analysis from meteorological stations

Using 14 weather stations in the CAA, a total of 625 ROS events were identified, of which 265 were classified as ROS $_{rain}$, 174 as ROS $_{rain/drizzle}$, 31 as ROS $_{mix}$ and 155 as ROS $_{Unclass}$ for the 1984-2014 period. Figure 2A shows the distribution of ROS classes across the CAA and highlights a higher occurrence of ROS at lower latitudes (< 70°N). High latitude stations (> 70°N) registered less than 150 ROS events between 1984 and 2014 (i.e., ~22% of all ROS events identified). The highest number of ROS occurrences was seen at Hall Beach (HB), with more than 100 events throughout the period. This variability between northern and southern arctic stations could be explained by oceanic currents, warmer seasonal temperatures and associated increased moisture, but no data are available to validate such assumption.

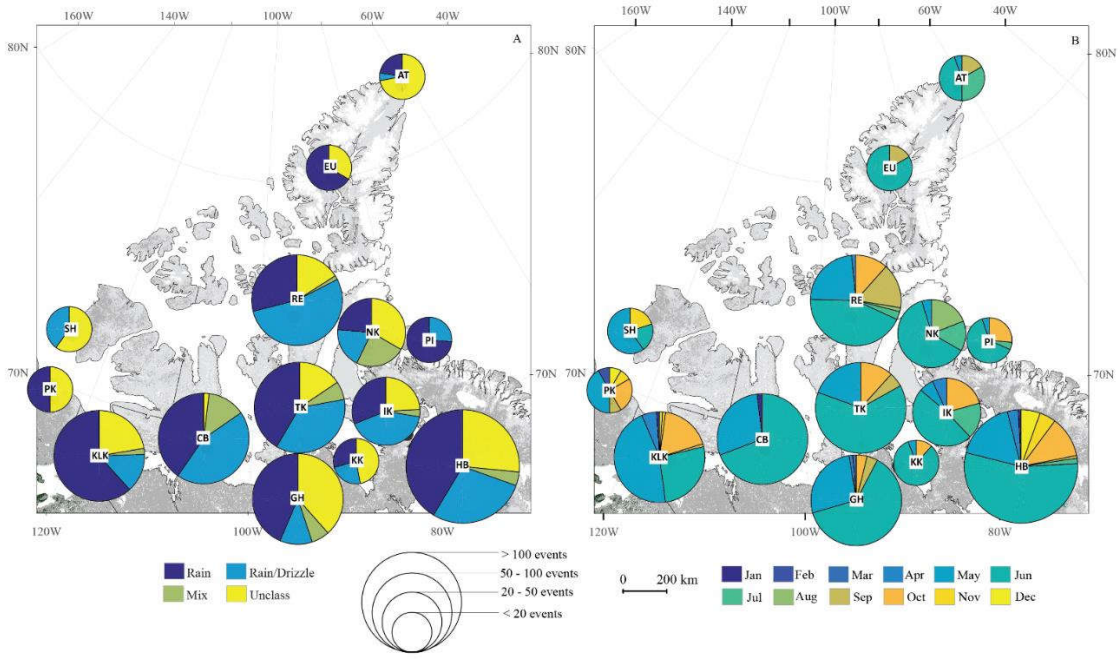

Figure 2. Monthly distribution of ROS events between 1985 and 2013 in the CAA. Pie-chart size represents the number of ROS events and colors represent different months.

We extracted ROS events from the meteorological station database for four periods: fall (~ September 20 to ~ December 20), winter (~ December 20 to ~ March 20), spring (~ March 20 to ~June 20) and summer (~ June 20 to September 20). The temporal occurrences for each of these periods are shown in Figure 3. ROS events are unevenly distributed through the year. Indeed, the spring ROS accounts more than 75% of the total occurrences, while ~14% of the events occur in fall, ~8% during summer and less than 1% in winter. Of relevance, the month of June accounts for more than half of the ROS recorded at all stations throughout the study period. One should note that 13 of the 14 stations received at least one ROS event during spring, whereas five to 11 stations were affected during fall, and one to four during winter. During the fall and winter periods, ROS events have a significant impact on snow metamorphism and stratigraphy with the formation of an ice crust

near the surface that affects energy transfer (Colbeck, 1980). Although the metamorphism processes can be observed during spring, the sustained warm air temperatures will promote a transition between the pendular and funicular regimes, leading to deeper water percolation. The modification of snow structure and formation of ice crusts throughout the year can lead to unfavorable grazing conditions for various ungulate species (Sokolov et al., 2016; Ouellet et al. 2017; Langlois et al. 2017).

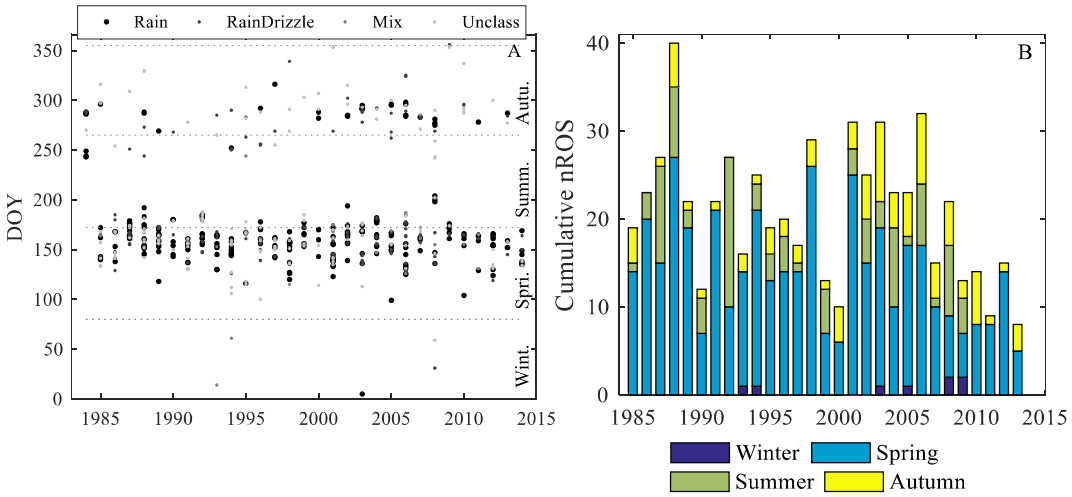

Figure 3. Annual vs. monthly distribution of ROS events (for each class) during the analysis period for all stations combined (A) and seasonal distribution and evolution of ROS events for all stations combined (B).

The results of seasonal trend for fall, winter, spring and summer do not suggest a significant trend due to high year-to-year variability, it is interesting that spring and summer seasons experience fewer ROS events (perhaps linked to a reduced snow cover duration), while an increase in event occurrence is seen during fall and winter. This is relevant for various applications, such as caribou grazing conditions since November-March is the migration period and is a critical time for calf survival.

Interannually ROS distribution by station does not appear to have followed any trend since 1985 (Fig. 4), despite a rise in air temperature. We also investigated potential trends by precipitation class (ROS_{rain}, $ROS_{rain/drizzle}$, ROS_{mix} and $ROS_{Unclass}$) (Fig. 4), and the results did not reach statistical significance. Although an increase in temperature of about 2°C has been clearly visible since 1984 (Fig. 4B), no statistically significant trend can be seen in ROS occurrence. As expected, we see a predominance of low latitude stations (from TK to KLK; i.e., <70N) in the interannually distribution of global ROS (Fig. 4A) and for the ROS_{rain} condition, while we can see a predominance of higher latitude stations (from SH to AT, i.e., >70N) for $ROS_{rain/drizzle}$. For other conditions, no trend can be distinguished (Fig. 4 E, F). Although there is no notable trend, significant variability can be observed where peaks in occurrence can be linked to main northern climate modes. It appears (not shown) that the negative periods of the Arctic Oscillations (as well as the very similar North Atlantic Oscillations, http://www.cpc.noaa.gov) are well synchronized with the observed higher numbers of observed ROS events (>20/yr) between 1984 and 2010. These results agree with Cohen et al., 2015 analysis derived from reanalysis-based study.

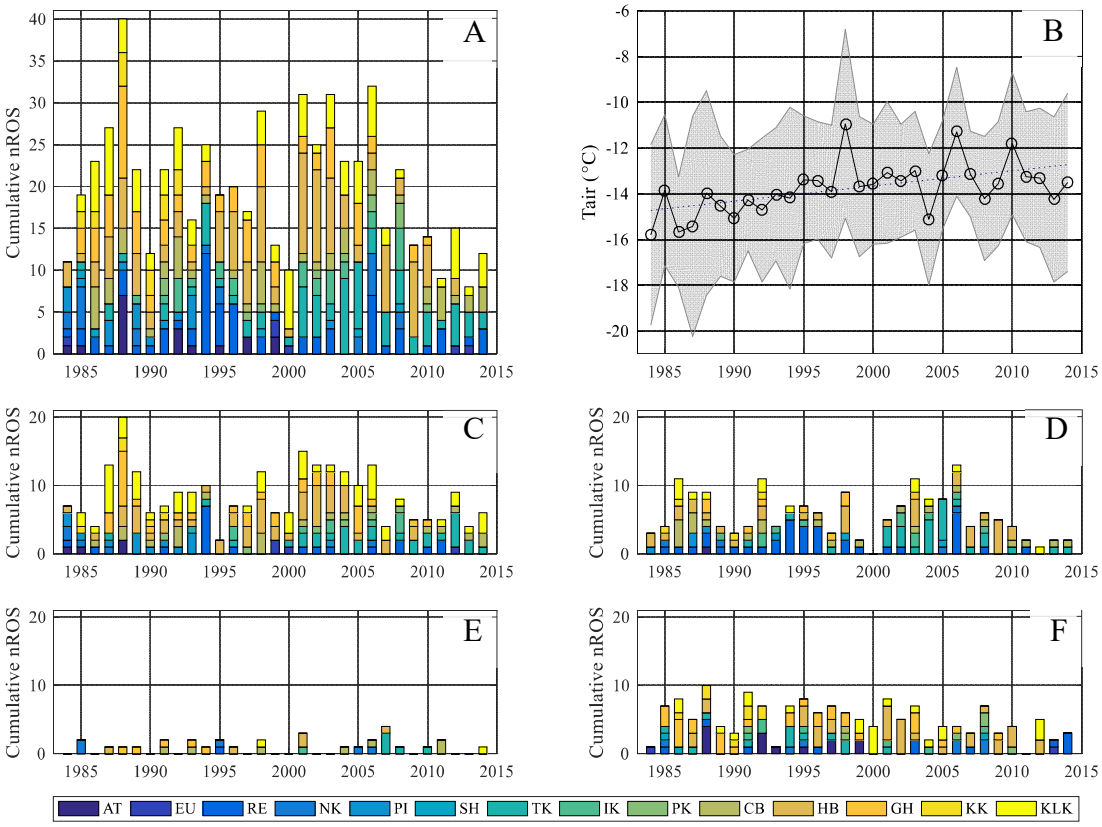

Figure 4. Temporal yearly ROS distribution by station between 1984 and 2014, using all event types (A), for ROS $_{rain}$ (C), ROS $_{rain/drizzle}$ (D), ROS $_{mix}$ (E) and ROS $_{Unclass}$ (F) separately. These figures are compared to winter air temperature (annual mean from ECCC stations) trends for all stations combined during same period (B).

The distinction between different precipitation conditions is important from a microwave radiometry perspective. The presence of rain, drizzle or snow in and on snowpack have a different impact on T_B. In fact, mixed precipitations have a smaller impact on T_B (i.e., GRP), and are thus harder to detect using our algorithm. Furthermore, the relationship between precipitation amount and air temperature did not follow any specific spatial distribution. In Figure 5 we can see this relationship where ROS $_{rain}$ were observed at temperatures above 0°C and the precipitation amounts are concentrated around 2 mm except for KK and NK (Fig. 5A). For the ROS $_{rain/drizzle}$ condition, the values are centered around 0°C, and precipitation amounts remained under 5 mm for all stations (Fig. 5B), while the relationship is more scattered for ROS $_{mix}$ and ROS $_{Unclass}$ conditions with air temperature values varying between -10°C and +5°C and precipitation amount values varying from 0.5 to 2 mm. For ROS $_{Unclass}$, a predominance of small average values of precipitation amounts and air temperatures below 0°C can be seen.

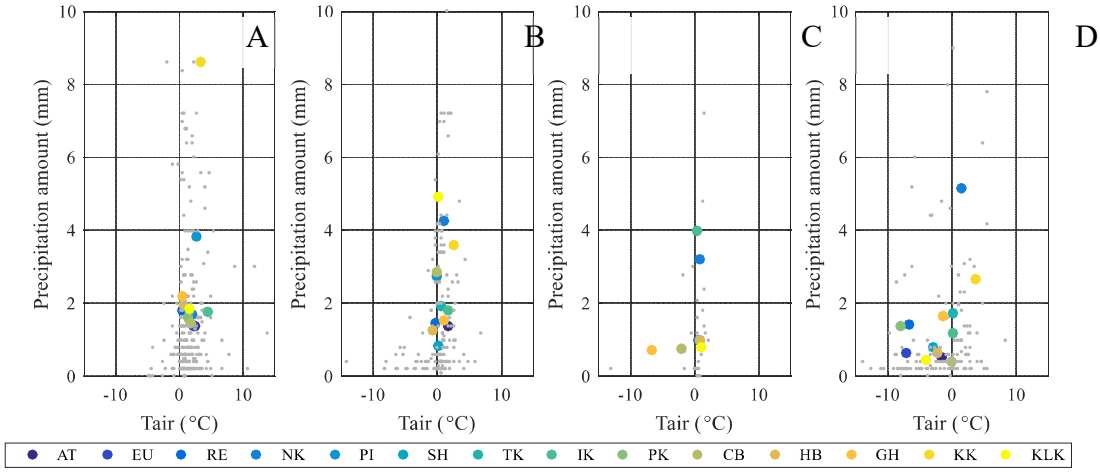

Figure 5. Relationship between air temperature and precipitation amount for rain conditions (A), for rain and drizzle conditions (B), for mix conditions (C) and for unclass conditions (D), between 1984 and 2014. The colored dots correspond to station averages and the grey points are data for all stations combined for different ROS classes.

Figure 6 shows the distribution of precipitation rate (in $mm.h^{-1}$) for each ROS condition. Most ROS (irrespective of ROS condition) are classified with small precipitation rates (i.e., <1 $mm.h^{-1}$). It is important to distinguish rate and amount of precipitation. Precipitation rate is derived from the accumulated precipitation and time duration recorded at the meteorological station so that the derived rate value is an hourly approximation (due to a lack of robust data of ROS time duration), and not a direct measurement. Given the rather cold temperatures and low humidity at which ROS occurs in the Arctic, the precipitation rates remain rather small. The precipitation rate itself can be classified into 5 categories (<0.5 mm; 0.5 to 1 mm; 1 to 2 mm; 2 to 5 mm and >5 mm). It is possible to see a predominance of weak precipitation rates (i.e., rate <0.5 $mm.h^{-1}$), which corresponds to 71.3%, 62.6% and 77.4% of all ROS events for ROS_{rain}, $ROS_{rain/drizzle}$ and ROS_{mix}, respectively (this statistic is not available for $ROS_{Unclass}$ due to a lack of data).

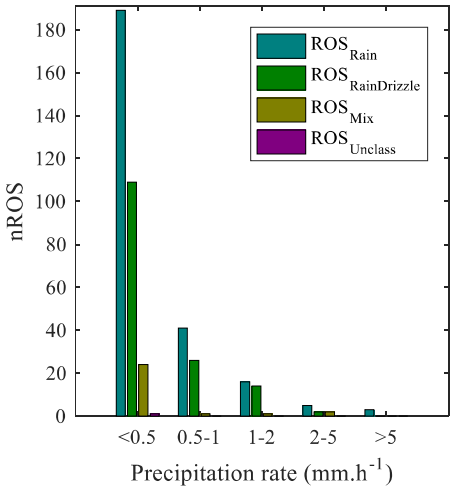

Figure 6. Number of ROS event (nROS) per classes of precipitation rate in $mm.h^{-1}$, for ROS_{rain}, $ROS_{rain/drizzle}$, ROS_{mix} and $ROS_{Unclass}$ conditions, for all stations combined across CAA.

Passive microwave detection using GPR approach

It remains unclear what minimum precipitation amount or rate will lead to a ROS detection using our passive microwave algorithm. As explain in section above, no specific trends are seen and that the omission of small events will remain a source of error. In Figure 7A we thus present the relationship between the GRP threshold and number of ROS detected. One can see a decrease in detected events with a decreasing GRP threshold over a range of -1 to -20 with a more significant decrease between thresholds of 1 (threshold of Dolant et al., 2016) to -5 (*i.e.* when GRP = 1, nROS = 7688 in ascending orbit and 4936 for descending orbit, whereas when GRP = -5, nROS = 289 for ascending orbit and 167 for descending orbit).

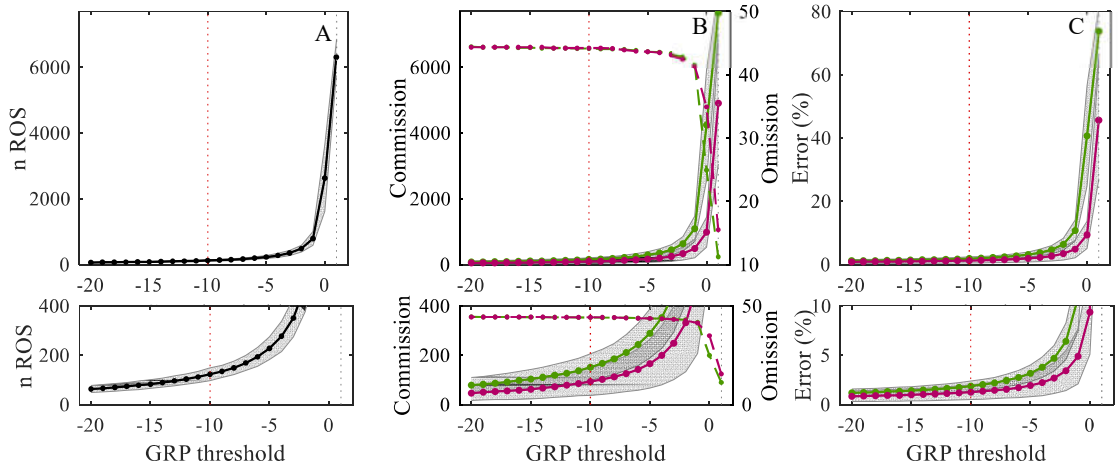

Figure 7. Average number of ROS (nROS) detected as a function of different GRP thresholds for all stations and for both ascending and descending orbits (A). Total number of commission and omission of detection (B) and error evolution (in percent; C) for GRP threshold variation, in subplots B and C, the line corresponds to commission and the dotted line corresponds to omission, the green line corresponds to ascending orbit and the purple line to descending orbit. For all subplots, the grey area represents the standard deviation. For A, B, C the dashed line in grey correspond at threshold of Dolant et al., 2016 and the red dashed line corresponds at new threshold.

We investigated the sensitivity of the detection algorithm to the threshold by comparing omission and commissions over the same range of GRP thresholds. Commissions occur when a ROS is detected by the algorithm, but not observed at the station (commission by the algorithm). Omissions occur when the opposite is observed (ROS seen at station but not detected by the algorithm). The best ROS event detection (perfect match between inventory date and detection date) is achieved when using a low GRP threshold (around -1), but that will lead to a significant increase in commissions (Fig. 7B). Figure 7C also suggests that most of the errors come from commissions and that the total error (omission + commission, see Fig. 7C) stabilizes at -10, where total error is equal to 1.9 for ascending orbit and 1.3 for descending orbit (i.e. omission is around 44 for each orbit and commission is around 152 for ascending orbit and 93 for descending orbit), which becomes the updated threshold for ROS detection. It also agrees with the nROS observed at the stations (Fig. 7A).

DISCUSSION

The main uncertainties using the available ECCC meteorological information are the precipitation timing and amount. First, the satellite passes are fixed, and no information is available on rain amount at a specific time (only daily cumulated values are available). For instance, a satellite can pass overhead during a ROS without detecting it if insufficient water is present to create the T_B reversal between 19 and 37 GHz at horizontal polarization. This would result in an 'omission' from

the algorithm. As such, the dataset cannot be used as an absolute reference for validation of the GRP approach, but it provides a collection of rain conditions and T_B responses to evaluate the sensitivity of the threshold (Figs. 7A and 7B). A true validation and adjustment of the approach would require hourly precipitation phase data, which will be available in Cambridge Bay in 2018 (disdrometer installation planned). Even though these uncertainties are present, this work allows a good framework of ROS detection measurement, and thus a good overview of this phenomenon throughout the CAA area. Other studies will evaluate the link between meteorological conditions, ROS intensity and impact intensity in snow structure and in environment. Nonetheless, our results highlight the best compromise for detection accuracy, where a threshold of -10 suggests a good equilibrium between omissions and commissions. One could reduce the threshold to increase the number of perfect detection matches, however this would translate into an increase in commissions, thereby reducing the overall accuracy. Moreover, this threshold could be adjustable for different applications and different levels of application (e.g., increasing the threshold to -5, where here more than 200 ROS could be detected, for civil security in Inuit communities (Berkes and Jolly, 2001)).

The periods for which visual observations are available is another source of uncertainty. However, the datasets included several gaps in these periods, occasionally with no observations for several consecutive days, which meant that the algorithm had no reference data. Consequently, it is hard to conclude on spatial and/or temporal event occurrence trends using this dataset.

CONCLUSION

This study presented ROS occurrences at 14 stations across the Arctic between 1984 and 2014 to evaluate the robustness of the GRP approach developed by Dolant et al., 2016 in an Arctic context. The basic statistical analysis highlighted a total of 603 ROS events throughout the study period (1984-2014), dominated by event occurrences at lower latitude stations. Three periods were studied separately and results show that despite no significant trends in the cumulated yearly occurrence, an increase is seen in the fall and winter ROS events.

We used the ROS inventory dataset to evaluate the performance and sensitivity of the GRP threshold developed by Dolant et al. (2016). Results suggest using a different threshold to differentiate between pure rain events and mixed precipitations with GRP thresholds of -15 and -10, respectively. Those thresholds also appear to match with the lowest detection error computed with omissions and commissions. Intuitively, the next step is to compute binary images of detected ROS across the CAA, and evaluate yearly anomalies in event occurrence (e.g., links to El Nino and Arctic Oscillation). Furthermore, the remote sensing product will also allow a better understanding of the various processes that can trigger an ROS. For instance, binary maps of event occurrences could be compared to sea proximity and polynya occurrence and evaluate future spatio-temporal trends of ROS across the Arctic.

REFERENCES

Berkes F, Jolly D. 2001, Adapting to climate change: social-ecological resilience in a Canadian western Arctic community. *Conservation Ecology*, **5**: 18. doi: 10.5751/ES-00342-050218.

Bokhorst S, Pedersen SH, Brucker L, *et al*. 2016. Changing Arctic snow cover: A review of recent developments and assessment of future needs for observations, modelling and impacts. *Ambio*, **45**: 516-537. doi: 10.1007/s13280-016-0770.

Brown RD, Braaten RO. 1998. Spatial and temporal variability of Canadian monthly snow depths, 1946-1995. *Atmosphere-Ocean,* **36**: 37-45.

Brown RD, Mote PW. 2009. The response of Northern Hemisphere snow cover to a changing climate. *Journal of Climate*, **22**: 2124-2145. doi: 10.1175/2008JCLI2665.1.

Brown R, Derksen C, Wang L. 2010. A multi-data set analysis of variability and change in Arctic spring snow cover extent, 1967–2008. *Journal of Geophysical Research*, **115**: D16111. doi:10.1029/2010JD013975.

Chen W, Russell DE, Gunn A, Croft B, Chen WR, Fernandes R, Zhao H, Li J, Zhang Y, Koehler K, Olthof I, Fraser RH, Leblanc SG, Henry GR, White RG, Finstad GL. 2013. Monitoring

habitat condition changes during winter and pre-calving migration for Bathurst Caribou in northern Canada. *Biodiversity*, **14**: 36-44.
Cohen J, Ye H, Jones J. 2015. Trends and variability in rain-on-snow events, *Geophysical Research Letters.,* **42.** doi:10.1002/2015GL065320.
Colbeck S. 1980. Thermodynamics of snow metamorphism due to variations in curvature. *Journal of Glaciology,* **26**: 291-301.
Colton MC, Poe GA. 1999. Intersensor Calibration of DMSP SSM/I's: F-8 to F-14, 1987-1997. *IEEE Transactions on Geoscience and Remote Sensing,* **37**: 418-439.
Comiso JC. 2014. Sea Ice Concentration and Extent. *Encyclopedia of Remote Sensing,* 727-743.
Cullather RI, Lim Y-K, Boisvert LN, Brucker L, Lee JN, Nowicki SMJ. 2016. Analysis of the warmest Arctic winter, 2015-2016. *Geophysical Research Letters*, **43**. doi:10.1002/2016GL071228.
Derksen C, Smith SL, Sharp M, Brown L, Howell S, Copland L, Mueller DR, Gauthier Y, Fletcher CG, Tivy A, Bernier M, Bourgeois J, Brown R, Burn CR, Duguay C, Kushner P, Langlois A, Lewkowicz AG, Royer A, Walker A. 2012. Variability and change in the Canadian cryosphere. *Climatic change,* **11**: 59-88.
Derksen C, Brown R. 2012. Spring snow cover extent reductions in the 2008–2012 period exceeding climate model projections. *Geophysical Research Letter,* **39**, 6p.
Dethloff K, Rinke A, Benkel A, Køltzow M, Sokolova E, Kumar Saha S, Handorf D, Dorn W, Rockel B, Von Storch H, Haugen JE, Røed LP, Roeckner E, Christensen JH, Stendel M. 2006. A dynamical link between the Arctic and the global climate system. *Geophysical Research Letters*, **33**: L03703. doi:10.1029/2005GL025245.
Dolant C*,* Langlois A*,* Montpetit B*,* Brucker L*,* Roy A*,* Royer A. 2016. Development of a rain-on-snow detection algorithm using passive microwave radiometry. *Hydrological Processes,* **30***:* 3184–3196.
Domine F, Barrere M, Sarrazin D. 2016. Seasonal evolution of the effective thermal conductivity of the snow and the soil in high Arctic herb tundra at Bylot Island, Canada. *Cryosphere*, **10**: 2573-2588.
Grenfell TC, Putkonen J. 2008. A method for the detection of the severe rain-on-snow event on Banks Island, using passive microwave remote sensing. *Water Resources Research*, **44**: W03425. doi: 10.1029/2007WR005929.
Holland MM, Serreze MC, Stroeve J, 2010. The sea ice mass budget of the Arctic and its future change as simulated by coupled climate models. *Climate Dynamics*, **34**: 185–200.
IPCC. 2013. Climate Change 2013: The Physical Science Basis. Contribution of Working Group I to the Fifth Assessment Report of the Intergovernmental Panel on Climate Change [Stocker TF, Qin D, Plattner G-K, Tignor M, Allen SK, Boschung J, Nauels A, Xia Y, Bex V, Midgley PM. (eds.)]. *Cambridge University Press, Cambridge, United Kingdom and New York, NY, USA*, 1535 pp.
IPCC. 2014. Climate Change 2014: Impacts, Adaptation, and Vulnerability. Part A: Global and Sectoral Aspects. Contribution of Working Group II to the Fifth Assessment Report of the Intergovernmental Panel on Climate Change [Field CB, Barros VR, Dokken DJ, Mach KJ, Mastrandrea MD, Bilir TE, Chatterjee M, Ebi KL, Estrada YO, Genova RC, Girma B, Kissel ES, Levy AN, MacCracken S, Mastrandrea PR, White LL (eds.)]. *Cambridge University Press, Cambridge, United Kingdom and New York, NY, USA*, 1132 pp.
IPCC. 2014. Climate Change 2014: Impacts, Adaptation, and Vulnerability. Part B: Regional Aspects. Contribution of Working Group II to the Fifth Assessment Report of the Intergovernmental Panel on Climate Change [Barros VR, Field CB, Dokken DJ, Mastrandrea MD, Mach KJ, Bilir TE, Chatterjee M, Ebi KL, Estrada YO, Genova RC, Girma B, Kissel ES, Levy AN, MacCracken S, Mastrandrea PR, White LL (eds.)]. *Cambridge University Press, Cambridge, United Kingdom and New York, NY, USA*, pp. 688.
IPCC. 2014. Climate Change 2014: Synthesis Report. Contribution of Working Groups I, II and III to the Fifth Assessment Report of the Intergovernmental Panel on Climate Change [Core Writing Team, Pachauri RK, Meyer LA (eds.)]. IPCC, Geneva, Switzerland, 151 pp.
Johnson CA, Neave E, Blukacz-Richards A, Banks SN, Quesnelles PE. 2016. Knowledge assessment (community and scientific) to inform the identification of critical habitat for Peary

caribou, *Rangifer tarandus pearyi*, in the Canadian Arctic. *Environment and Climate Change Canada, Science and Technology, Ottawa, Ontario, Canada.*
Klos PZ, Link TE, Abatzoglou JT. 2014. Extent of the rain-snow transition zone in the western U.S. under historic and projected climate. *Geophysical Research Letters*, **41**: 4560–4568.
Knowles K, Njoku EG, Armstrong R, Brodzik M. 2000. Nimbus-7 SMMR Pathfinder Daily EASE-Grid Brightness Temperatures, Version 1. *Boulder, Colorado USA, NASA National Snow and Ice Data Center Distributed Active Archive Center.*
Langlois A, Johnson CA, Montpetit B, Royer A, Blukacz-Richards EA, Neave E, Dolant C, Roy A, Arhonditsis G, Kin DK, Kaluskar S, Brucker L. 2017. Detection of rain-on-now (ROS) events and ice layer formation using passive microwave radiometry: A context for Peary caribou habitat in the Canadian Arctic. *Remote Sensing of Environment*, **189**: 84-95.
Liebe H. 1989. MPM-An atmospheric millimeter-wave propagation model. *International Journal of Infrared and Millimeter Waves*, **10**: 631-650.
Liston GE, Hiemstra CA. 2011. The Changing Cryosphere: Pan-Arctic Snow Trends (1979–2009). *American Meteorological Society.*
L'hôte Y, Chevallier P, Coudrain A, Lejeune Y, Etchevers P. 2005. Relationship between precipitation phase and air temperature: comparison between the Bolivian Andes and the Swiss Alps. *Hydrological Sciences Journal*, **50**: 989-997.
Mazurkiewicz AB, Callery DG, McDonnell JJ. 2008. Assessing the controls of the snow energy balance and water available for runoff in a rain-on-snow environment. *Journal of Hydrology,* **354**: 1-14.
Mesinger F, DiMego G, Kalnay E, Mitchell K, Shafran PC, Ebisuzaki W, Jović D, Woollen J, Rogers E, Berbery EH, Ek MB, Fan Y, Grumbine R, Higgins W, Li H, Lin Y, Manikin G, Parrish D, Shi W. 2006. North American Regional Reanalysis. *Bulletin of the American Meteorological Society*, **87**: 343-360.
Montpetit B, Royer A, Roy A, Langlois A, Derksen C. 2013. Snow microwave emission modeling of ice lenses within the snowpack using the microwave emission model for layered snowpack (MEMLS). *IEEE Transactions on Geoscience and Remote Sensing.*
Montpetit B. 2015. Analyse de la modélisation de l'émission multifréquence micro-onde des sols et de la neige, incluant les croutes de glace à l'aide du modèle Microwave Emission Model of Layered Snowpacks (MEMLS). *Ph.D. thesis, Université de Sherbrooke, Département de Géomatique Appliquée,* May 2015, 188p.
Ouellet F, Langlois A, Johnson CA, Richards A, Royer A. 2017. Spatialization of the SNOWPACK Snow model in the Canadian Arctic for Peary Caribou Winter Grazing Condition Assessment. *Physical Geography*, **38**: 143-158.
Pradhanang SM, Frei A, Zion MS, Schneiderman EM, Steenhuis TS, Pierson D. 2012. Analysis of Rain-on-snow Runoff Events in New York. *69th Eastern Snow Conference, Frost Valley YMCA, Claryville, New York, USA.*
Pradhanang SM, Frei A, Zion M, Schneiderman EM, Steenhuis TS, Pierson D. 2013. Rain-on-snow runoff events in New York. *Hydrological Processes*, **27**: 3035-3049.
Pulliainen J, Grandell T, Hallikainen J. 1999. Hut snow emission model and its applicability to snow water equivalent retrieval. *IEEE Transactions on Geoscience and Remote Sensing*, **37**: 1378-1390.
Putkonen J. 1998. Soil thermal properties and heat transfer processes near Ny Alesund, north western Spitsbergen, Svalbard. *Polar Research*, **17**: 165–179.
Putkonen J, Roe G. 2003. Rain-on-snow events impact soil temperatures and affect ungulate survival. *Geophysical Research Letters*, **30**: 1188.
Rennert KJ, Roe G, Putkonen J, Bitz CM. 2009. Soil Thermal and Ecological Impacts of Rain on Snow Events in the Circumpolar arctic. *Journal of Climate*, **22**: 2302-2315.
Romanovsky VE, Smith SL, Christiansen HH. 2010. Permafrost Thermal State in the Polar Northern Hemisphere during the International Polar Year 2007–2009: A Synthesis. *Permafrost and Periglacial Processes*, **21**: 106–116.
Roy A, Royer A, Wigneron JP, Langlois A, Bergeron J, Cliche P. 2012. A simple parameterization for boreal forest radiative transfer model at microwave frequencies. *Remote Sensing of Environment,* **124**: 371-383.

Serreze MC, Barrett AP, Stroeve JC, Kinding DN, Holland MM. 2009. The emergence of surface-based Arctic amplification. *The Cryosphere*, **3**: 11-19.
Serreze MC, Barry RG. 2011. Processes and impacts of Arctic amplification: A research synthesis. *Global and Planetary Change*, **77**: 85-96.
Steele M, Ermold W, Zhang J. 2008. Arctic Ocean surface warming trends over the past 100 years, *Geophysical Research Letters*, **35**: L02614. doi:10.1029/2007GL031651.
Sokolov AA, Sokolova NA, Ims RA, Brucker L, Ehrich D. 2016. Emergent Rainy Winter Warm Spells May Promote Boreal Predator Expansion into the Arctic. *Arctic*, **69**: 121. doi:10.14430/arctic4559.
Trenberth, KE, Jones PD, Ambenje P, Bojariu R, Easterling D, Klein Tank A, Parker D, Rahimzadeh F, Renwick JA, Rusticucci M, Soden B, Zhai P. 2007. Chapter 3, Observations: Surface and Atmospheric Climate Change. In: Climate Change 2007: The Physical Science Basis. Contribution of Working Group I to the Fourth Assessment Report of the Intergovernmental Panel on Climate Change [Solomon S, Qin D, Manning M, Chen Z, Marquis M, Averyt KB, Tignor M, Miller HL (eds.)]. *Cambridge University Press, Cambridge, United Kingdom and New York, NY, USA.*
Trenberth KE. 2011. Changes in precipitation with climate change. *Climate Research*, **47**: 123–138.
Wentz FJ, Spencer RW. 1988. SSM/I Rain Retrievals within a Unified All-Weather Ocean Algorithm. *American Meteorological Society,* **55**: 1613-1627.
Wentz FJ. 1997. A well-calibrated ocean algorithm for special sensor microwave/imager. *Journal of Geophysical Research,* **10**: 8703-8718.
Wentz FJ. 2013. SSM/I Version-7 Calibration Report*. Remote Sensing Systems Technical Report*, 46p.
Winton M. 2006. Does the Arctic sea ice have a tipping point? *Geophysical Research Letters*, **33**: 5p.